Primary Human Ligament Fibroblast Adhesion and Growth on 3D-Printed Scaffolds for Tissue Engineering Applications

Jean-Gabriel Lacombe [1,2,3], Megan E. Cooke [1,2,3], Hyeree Park [4], Suliman Mohammed Alshammari [1,3,5], Rahul Gawri [1,2,3], Showan N. Nazhat [4], Paul A. Martineau [1,3] and Derek H. Rosenzweig [1,2,3,*]

1   Division of Orthopaedic Surgery, McGill University, Montreal, QC H3A 1A1, Canada;
    jean-gabriel.lacombe@mail.mcgill.ca (J.-G.L.); megan.cooke@mail.mcgill.ca (M.E.C.);
    suliman.alshammari@mail.mcgill.ca (S.M.A.); rahul.gawri@mcgill.ca (R.G.);
    paul.martineau@mcgill.ca (P.A.M.)
2   Injury, Repair and Recovery Program, Research Institute of McGill University Health Centre,
    Montreal, QC H3A 1A1, Canada
3   Department of Experimental Surgery, McGill University, Montreal, QC H3A 1A1, Canada
4   Department of Mining and Materials Engineering, McGill University, Montreal, QC H3A 0C5, Canada;
    hyeree.park@mail.mcgill.ca (H.P.); showan.nazhat@mcgill.ca (S.N.N.)
5   Orthopaedic Department, Imam Abdulrahman Bin Faisal University (IAU), Dammam 34212, Saudi Arabia
*   Correspondence: derek.rosenzweig@mcgill.ca; Tel.: +1-(514)-934-1934 (ext. 45575)

Abstract: The current gold standard technique for the treatment of anterior cruciate ligament (ACL) injury is reconstruction with a tendon autograft. These treatments have a relatively high failure and re-rupture rate and are associated with early-onset osteoarthritis, developing within two decades of injury. Furthermore, both autografting and allografting come with several drawbacks. Tissue engineering and additive manufacturing present exciting new opportunities to explore 3D scaffolds as graft substitutes. We previously showed that 3D-printed scaffolds using low-cost equipment are suitable for tissue engineering approaches to regenerative medicine. Here, we hypothesize that Lay-Fomm 60, a commercially available nanoporous elastomer, may be a viable tissue engineering candidate for an ACL graft substitute. We first printed nanoporous thermoplastic elastomer scaffolds using low-cost desktop 3D printers and determined the mechanical and morphological properties. We then tested the impact of different surface coatings on primary human ACL fibroblast adhesion, growth, and ligamentous matrix deposition in vitro. Our data suggest that poly-L-lysine-coated Lay-Fomm 60 scaffolds increased ligament fibroblast activity and matrix formation when compared to uncoated scaffolds but did not have a significant effect on cell attachment and proliferation. Therefore, uncoated 3D printed Lay-Fomm 60 scaffolds may be viable standalone scaffolds and warrant further research as ligament tissue engineering and reconstruction grafts.

Keywords: 3D printing; scaffolds; anterior cruciate ligament; tissue engineering; low-cost; human fibroblasts; ligament reconstruction

1. Introduction

The anterior cruciate ligament (ACL) is one of the most frequently injured structures during sporting or high-impact activities [1]. It is a major contributor to knee joint stability and is responsible for the passive restraint of anterior translation of the tibia with respect to the femur [2–4]. Anterior cruciate ligament (ACL) tears in the knee are among the most common soft tissue orthopedic injuries, with close to 250,000 cases occurring annually in Canada and the USA alone [5]. If left untreated, ACL tears can lead to meniscal tears and accelerated osteoarthritis resulting from altered biomechanics of the knee joint [6,7]. Interestingly, ACL tears occur over 50% of the time at the enthesis—a transition zone of non-calcified and calcified fibrocartilage tissue connecting the ligament to the bone [8]. The ACL has a limited self-healing capacity; partial tears lack the vascularization necessary for

spontaneous regeneration while complete tears are physically separated and lack stimuli and scaffolding required to regenerate [9–14]. As a result, surgical reconstruction by grafting tissue from the hamstrings or patellar tendon is the current gold standard of care for ACL injuries [15]. However, surgical treatment is costly and has a risk of graft donor site morbidity and unfavorable outcomes, including a risk of post-traumatic osteoarthritis within two decades of surgery [16–19]. Furthermore, incomplete or irregular healing of tissue grafts used in ACL reconstruction can result in abnormal knee biomechanics [20,21].

Tissue engineers are working to develop ligament substitutes to address the shortcomings associated with traditional ACL surgical techniques. Ideal tissue-engineered ligament scaffolds will mimic the mechanical properties of the native ACL while enabling cell attachment for tissue regeneration and maturation [22]. In designing ACL scaffolds, important design requirements include microstructure, external geometry, degradation characteristics, and mechanical competence, as well as porosity and interconnectivity [23,24]. One challenging aspect of designing ACL scaffolds is the fabrication of constructs that mimic the complex anisotropic properties of the native tissue [25]. Furthermore, the cross-sectional geometry of the ACL changes with the angle of flexion, and its area is generally larger in the anterior–posterior direction.

Fused deposition modelling, the most common type of 3D printing, is a fabrication process where 3D computer-generated models are built layer by layer from polymer filaments [26]. The technique has been used for a variety of applications due to the ability to produce geometries and parts that are too complex for traditional subtractive manufacturing processes [27,28]. Three-dimensional printing of polymeric scaffolds can generate mechanically competent macroporous structures that can act as templates for tissue regeneration [26,29]. A wide range of polymeric materials has been used for fused deposition modelling (FDM). This includes a variety of biocompatible and resorbable materials such as poly-L-lactic acid, polyurethane urea, and polycaprolactone that have been used to generate ligament/tendon-like scaffolds [30–33]. While additive manufacturing allows for the fabrication of scaffolds that more appropriately mimic the morphology and mechanical properties of the native tissue, cell attachment efficiency on these scaffolds is often low and may result in inefficient cell colonization [34–37]. Material surface modification such as plasma, laser, and chemical treatment, as well as protein coating are commonly used in order to improve cell attachment and promote more efficient scaffold colonization [38–41]. However, these techniques can be expensive, time-consuming, and difficult to reproduce [39–42].

Lay-Fomm 60, a thermoplastic polyurethane (TPU) copolymer with polyvinyl alcohol (PVA), can be manufactured via fused deposition modeling (FDM) before PVA is removed by washing in water to reveal a nanoporous, sponge-like TPU network. The resulting construct has been used in biofuel cell development [43], modeling of elastic tissues [44], and local drug delivery approaches [45]. We have also recently shown its compatibility and bone repair potential in vivo [30]. In this study, we generated low-cost, nanoporous thermoplastic elastomer scaffolds and tested the impact of various cell-adhesive coatings on primary human ligament fibroblast adhesion, growth, and ligament-like matrix deposition. Furthermore, mechanical and morphological properties of the scaffolds were investigated. We aimed to determine whether coating 3D-printed scaffolds could enhance primary ACL fibroblast adhesion and whether it would be pertinent to ACL graft substitutes.

2. Materials and Methods

2.1. Scaffold Fabrication

For the fabrication of 3D-printed scaffolds, 1.75-mm Lay-Fomm 60 filament (Matter-Hackers, Lake Forest, CA, USA) was purchased. The scaffolds (Figure 1) were designed using the SolidWorks CAD software (Version 23, Dassault Systèmes, SolidWorks Corporation, Waltham, MA, USA) and converted to the stereolithography (.stl) file format. The $5 \times 5 \times 0.7$ mm cuboid was converted to the RealFlight content format (.g3x) using the Cura 4.3.0 (Ultimaker, Utrecht, Netherlands) open-source 3D printer slicing software. Be-

fore printing, the Lay-Fomm filament was heated to 80 °C for 1 h and then placed in a desiccator for 30 min to remove moisture. The scaffolds were printed on a FlashForge Creator Pro 3D Desktop Printer (Flashforge, Los Angeles, CA, USA) with an extruding temperature of 220 °C, 90% infill density, and a 0.3 mm diameter nozzle. The print speed was 15 mm/s for the first layer and 25 mm/s for the ensuing layers, resulting in the total printing time of 9 minutes for each scaffold. After printing, the constructs were placed in double-distilled water at room temperature for 72 h and water was replaced every 24 h to wash out the polyvinyl alcohol (PVA) component. The PVA component was estimated to take up approximately 36% [30].
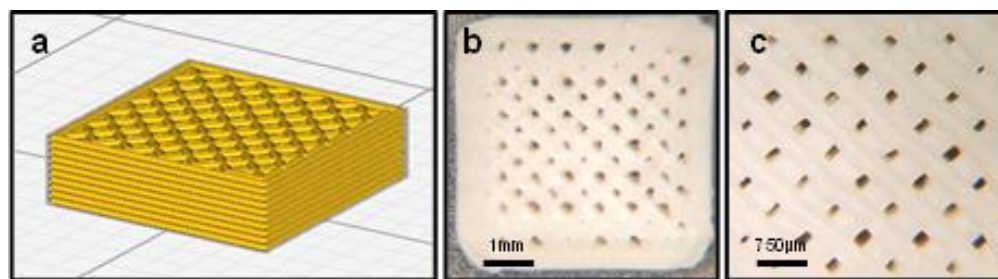

Figure 1. Scaffold design. (**a**) Scaffold sliced using the Ultimaker Cura 4.3.0 software. The scaffold was designed as a solid cube and printed with 90% infill density and a grid infill pattern. (**b**,**c**) Printed scaffold prior to washing in water.

2.2. Surface Coating of the Scaffolds

Once washed, the scaffolds were rinsed in 70% ethanol for 20 min and placed under UV light in a biosafety cabinet overnight. The sterile scaffolds were washed twice with PBS (Ca/Mg-free). Four different surface coating materials were applied on the Lay-Fomm scaffolds for evaluation: 0.2% bovine type B gelatin (MilliporeSigma, Burlington, VE, USA), 50 µg/mL rat tail collagen type I (Gibco, Billings, MT, USA), 0.01% and 0.001% poly-L-lysine (MilliporeSigma, Burlington, VE, USA), and 8 µg/mL bovine plasma fibronectin (MilliporeSigma, Burlington, VE, USA). The scaffolds were submerged in 250 µL of each coating material in a 48-well plate and incubated at room temperature for 2 h. The coatings were then aspirated, and the scaffolds were gently rinsed three times with sterile PBS to remove unbound material. All the scaffolds were left to air-dry for 15 min, and the plates were sealed with parafilm and stored at 4 °C overnight.

2.3. Isolation and Culture of Primary Human Ligament Fibroblasts

Human ACL samples were collected from the ACL reconstruction surgeries performed at the McGill University Health Centre. Patient samples were collected with consent under RI-MUHC-approved REB #2019-5390. The samples collected were from four donors with the age range of 20–26 (mean age, 23 years old). Two of the donors were women and two were men. The samples were collected into phosphate-buffered saline (PBS, Ca/Mg-free, pH 7.4, Gibco) and transported directly to the laboratory for cell isolation. The samples were then washed vigorously with sterile PBS supplemented with antibiotics (0.5 µg/mL amphotericin B (Gibco) and 200 µg/mL Primocin (Invivogen, San Diego, CA, USA)) and diced into 1–2 mm pieces. The tissue was digested overnight in collagenase-supplemented DMEM (standard growth medium: high-glucose Dulbecco's modified Eagle's medium (MilliporeSigma); 0.1 mM nonessential amino acids; 10 mM HEPES; 1 mM sodium pyruvate; 10% fetal bovine serum (MilliporeSigma); and 1% penicillin–streptomycin–glycine (Gibco), 1.5 mg/mL collagenase type II (Gibco)). The digest was passed through 100 µm and 70 µm filters sequentially (BD Biosciences, Mississauga, ON, Canada) and centrifuged at $500 \times g$ for 5 min. Fibroblasts were resuspended in 5 mL of the growth medium in a T-25 flask and cultured at 37 °C in a humidified cell culture incubator with 5% CO_2.

2.4. Cell Seeding and Culture on the Scaffolds

Confluent cells (between passages 3 and 4) were washed with sterile PBS, detached using 0.25% trypsin–EDTA (Gibco), and centrifuged at $500 \times g$ for 5 min. The cells were suspended in fresh culture media and seeded onto the scaffolds using a syringe as previously described [46]. Briefly, the passaged cells were placed in 5 mL syringes fitted with a four-way stopcock with a rotating collar (Navilyst Medical Inc., Marlborough, MA, USA) at a density of 2×10^5 cells/scaffold. The scaffolds were placed in the syringes and kept inside the culture incubator for 3 h, turning every 45 min to promote equal cell adhesion. The scaffolds were then transferred to a 48-well nonadherent cell culture plate and covered with the growth medium while the cells remaining in each syringe were counted to assess cell adhesion.

2.5. Mechanical Testing

Mechanical tests were performed as previously described [47]. Briefly, 25 cm pieces of the Lay-Fomm 60 filament (directly from the spool) were placed in double-distilled water for 72 h, and water was replaced every 24 h. Tensile testing of both washed and unwashed filament (N = 3) was performed using an MTS Mini-Bionix 858 (MTS; 14000 Technology Dr., Eden Prairie, MN, USA) controlled with the TestStar II 4.0C (MTS) software using an LCCD-100 load cell (Omegadyne, 800 Connecticut Ave., Suite 5N01, Norwalk, CT 08654, USA). Both the load and displacement data were recorded at 10 Hz. The displacement was set to a maximum of 95 mm and the test speed was set to 0.3 mm/s. All the tests were performed at a laboratory that was controlled for temperature ($22 \pm 1 \,°C$).

2.6. Scaffold Geometry

To characterize the scaffold geometry following printing, μCT analysis of the unwashed Lay-Fomm 60 scaffolds was performed using a Skyscan 1172 (Bruker, Kontich, Belgium) with a pixel size of 5 μm. The NRecon v.1.6.10.4 and CTAn v.1.16.4.1 software programs (Bruker) were used to reconstruct 3D volumes and perform quantitative analysis, respectively, as described previously [48]. Quantitative data were recorded for the entirety of the scaffold volume. The reported parameters were scaffold volume/ROI volume (SV/RV, %), scaffold surface area (SS, mm^2), average scaffold filament thickness (SF.Th, μm), pore size (SF.Sp, μm), and total porosity (Po.Tot, %).

2.7. Surface Morphology

Both the acellular and cell-seeded (day 14) scaffolds were imaged using scanning electron microscopy (SEM) (FEI Inspect F50 FE-SEM, FEI Company, Hillsboro, OR, USA). Briefly, the scaffolds were fixed for 10 min with 4% paraformaldehyde, rinsed with PBS, and subsequently dehydrated with 80%, 90%, and 100% ethanol for 10 min each. The samples then underwent critical point drying (Leica Microsystems EM CPD 030, Wetzlar, Germany) and platinum sputter coating (4 nm). Morphological characteristics of the scaffolds and the attached cells were observed using SEM with an acceleration voltage of 10 kV.

2.8. Gene Expression

Quantitative reverse transcriptase-mediated PCR (RT-qPCR) was performed on isolated primary human ACL fibroblasts at passage 0 to assess ligamentogenic gene expression. TRIzol™ (Invitrogen, Carlsbad, CA, USA) was used to extract RNA following the manufacturer's instructions, and the qScript reagent (Quantabio, Beverly, MA, USA) was used to reverse-transcribe 500 ng of RNA to cDNA.

Primers were used previously at our lab [48–50], and were derived from published validated studies, GAPDH [51], and all other ligament-related primers [52](Table 1, Life Technologies Inc., Carlsbad, CA, USA). Quantitative RT-PCR analysis was performed on a StepOnePlus Real Time PCR System (Applied Biosystems, Foster City, CA, USA) using the PerfeCTa SYBR Green detection reagent (Quantabio, Beverly, MA, USA). Amplification of collagen type I (COLIA1), collagen type III (COL3A1), tenascin C (TN-C), scleraxis (SCX),

and glyceraldehyde 3-phosphate dehydrogenase (GAPDH) was quantified (Table 2, Life Technologies Inc., Carlsbad, CA, USA). Expression was normalized to the housekeeping gene glyceraldehyde 3-phosphate dehydrogenase (GAPDH), and relative fold expression for each target gene was evaluated using the $\Delta\Delta^{CT}$ method. To ensure tendon/ligament gene expression, we used undifferentiated human bone marrow mesenchymal stem cells as the control (RoosterBio Inc., Frederick, MD, USA) at passage 0.

Table 1. RT-PCR product length, as well as Genbank's gene ID for the primers used for q-PCR (Life Technologies Inc., Carlsbad, CA, USA).

Target Gene	Product Length (bp)	Genbank's Gene ID
GAPDH	1978	NM_001170721
COLIA1	462	NM_001102599
COL3A1		
TN-C	1065	AL445645.10
SCX	1930	NG_053063.1

Table 2. Sequence of the forward and reverse primers used for q-PCR (Life Technologies Inc., Carlsbad, CA, USA).

Target Gene	Forward Primer (5′—3′)	Reverse Primer (3′—5′)
GAPDH	TCCCTGAGCTGAACGGGAAG	GGAGGAGTGGGTGTCGCTGT
COLIA1	GGTGATGCTGGTCCTGTTG	CATCGTGAGCCTTCTCTTGAG
COL3A1	CCCAGAACATCACATATCAC	CAAGAGGAACACATATGGAG
TN-C	ACCGTCTCTTCCGTCACTTCT	AACAACTTAGGACAATGCGTCT
SCX	AGAACACCCAGCCCAAACA	TCCTTGCTCAACTTTCTCTGGT

2.9. Cell Viability and Proliferation

Cell viability at days 7 and 14 was determined using a LIVE/DEAD™ assay (Invitrogen) prepared in sterile PBS according to the manufacturer's instructions. Images were captured using an Olympus IX81 inverted fluorescence microscope using a 4× objective with MAG Biosystems Software 7.5 (Photometrics, Tucson, AZ, USA).

Cellular metabolic activity at days 3, 7, and 14 was determined using an AlamarBlue™ assay (Thermo Fisher, Waltham, USA) prepared in serum-free Dulbecco's modified Eagle's medium according to the manufacturer's instructions. Briefly, the AlamarBlue™ dye was added to the media at 1:10 dilution, the cells were incubated at 37 °C for 4 h, and the samples' fluorescence was measured in 96-well plates using a Tecan M200 Pro plateFtels reader (Tecan, Mannedorf, Switzerland) at Ex 570 nm and Em 600 nm.

Following 14 days of culture, the scaffolds were gently rocked in 500 μL of 4 M guanidine hydrochloride (GuHCl) buffer supplemented with a complete protease inhibitor cocktail (Roche Holding AG, Basel, Switzerland) for 48 h at 4 °C. The DNA content for the coated and uncoated scaffolds was measured using a DNA Hoechst 33258 assay. All the GuHCl extracts were diluted 10-fold prior to analysis. The standard curve was generated using calf thymus DNA (Invitrogen, Carlsbad, CA, USA) supplemented with the same volume of diluted 0.4 M GuHCl as the samples. Hoechst 33258 (Molecular Probes, Thermo Fisher) was prepared according to the manufacturer's instructions (Thermo Fisher). The samples were analyzed in triplicate in a 96-well microplate using a Tecan M200 Pro plate reader (Tecan) at Ex 352 nm and Em 460 nm and 420 nm cut-off.

2.10. Immunofluorescence and Protein Analyses

The scaffolds of each coating type were treated with a permeabilization buffer (PBS, 1% BSA, 0.1% Triton-X100) for 45 min. The permeabilized samples were then incubated with antibodies against tenomodulin (1:200, Abcam, cat. No. ab203676, Cambridge, MA, USA) at room temperature for 1.5 h. The samples were washed three times in PBS and then incubated with Alexa Fluor 488 donkey anti-rabbit IgG (1:1000, Invitrogen, cat. No. A21306)

with Texas Red™-X Phalloidin (1:400, cat. No. T7471, Invitrogen) at room temperature for 1 h. The samples were washed with PBS and mounted using Fluoroshield with DAPI (Sigma, Kawasaki, Japan) and visualized on an EVOS M5000 microscope (Thermo Fisher).

Proteins were extracted by GuHCl as above. Protein concentration was quantified using a BCA Assay (Thermo Fisher) and 25 μg protein was precipitated overnight at $-20\,^{\circ}$C in nine volumes of 100% ethanol for each scaffold. The precipitates were recovered by centrifugation for 30 min at 4 °C. The pellets were washed with ice-cold 90% ethanol, dried, and dissolved in 25 μL 1× NuPage® LDS sample buffer (Invitrogen, Carlsbad, CA, USA). Twenty-five μg of the protein then underwent electrophoresis in a 4–20% gradient SDS-PAGE gel (Bio-Rad, Hercules, CA, USA) and were transferred to Amersham™ Protran® 0.2 μm nitrocellulose blotting membranes (GE Healthcare, Chicago, IL, USA). The membranes were first blocked for 1.5 h in 5% BSA and incubated for 24 h at 4 °C with mouse monoclonal antibodies against collagen type I (1:1000; Abcam, cat. No. ab6308, Cambridge, MA, USA). The nitrocellulose membranes were washed three times in TBS-T followed by incubation with an anti-mouse HRP-conjugated secondary antibody (1:1000, Santa Cruz Biotechnology, Dallas, TX, USA) for 45 min. The membranes were then washed three times in TBS-T for 10 min and developed using Western Lightning Plus-ECL (Perkin Elmer, Waltham, MA, USA) before imaging on an Image Quant LAS 4000 (GE Healthcare Bio-Sciences, Baie d'Urfe, QC, Canada). After imaging, the membranes were stripped, blocked in 5% BSA for 1.5 h, and reprobed with rabbit polyclonal antibodies against collagen type III (1:5000; Abcam, cat. No. Ab7778, Cambridge, MA, USA) at room temperature for 2 h. The membranes were then incubated with an anti-rabbit HRP-conjugated secondary antibody (1:5000, Santa Cruz Biotechnology, Dallas, TX, USA) for 1 h and developed as above. Lastly, the stripped membranes were blocked in 3% BSA for 1 h and probed with mouse monoclonal antibodies against alpha tubulin (1:5000; Abcam, cat. No. ab7291) at room temperature for 1 h. The membranes were then incubated with the anti-mouse HRP-conjugated secondary antibody (1:5000, Santa Cruz Biotechnology, Dallas, TX, USA) for 45 min.

2.11. Statistical Analysis

All the experiments were repeated at least three times (N = 3) and the measurements were performed in triplicate (N = 3). The results are expressed as the means ± SD. All the statistical analyses were performed comparing the various coated scaffolds to the uncoated control scaffolds using unpaired *t*-tests from at least three independent experiments. Significance was set at $p \leq 0.05$. The analyses were performed using Prism 6.0 (Graphpad Software, La Jolla, CA, USA).

3. Results

3.1. Mechanical Testing and Scaffold Characterization

We previously characterized some mechanical properties of the Lay-Fomm 60 filaments in terms of elastic limits and Young's modulus [30,52]. Here, we tested the mechanical properties of specific-geometry 3D-printed scaffolds. Representative stress–strain curves for washed and unwashed Lay-Fomm 60 tensile specimens are shown in Figure 2a. The ultimate tensile strength values were 2.07 ± 0.31 MPa and 13.69 ± 1.78 MPa for the washed and unwashed specimens, respectively. The strain at failure was 76.46 ± 31.08% for the washed specimens and 66.64 ± 18.98% for the unwashed specimens.

The 3D printing process generated scaffolds of consistent dry mass and dimensions (Table 3). The average dry mass of the three scaffolds analyzed was 88.3 ± 0.7 mg. Scaffold dimensions of 5 × 5 × 0.7 mm and the average SS area of 159.5 ± 2.2 mm^2 were recorded. Both μCT reconstruction and SEM (Figure 3) indicate the presence of nozzle friction since the printed scaffold pores were asymmetrical while the designed pores were of symmetric rectangular geometry. Despite nozzle friction, pore size was highly consistent and suitable for ligament fibroblasts to enter the top of the scaffold and penetrate and adhere to strut surfaces in the depth of the scaffolds. The average pore size (SF.Sp) was 271.7 ± 4.6 μm

while the average filament thickness (SF.Th) was 479.9 ± 10.7 μm. The SV/RV ratio was 60.7 ± 1.0% on average. The total porosity was 39.3 ± 1.0%, indicating that the scaffold fabrication process features high precision and accuracy.
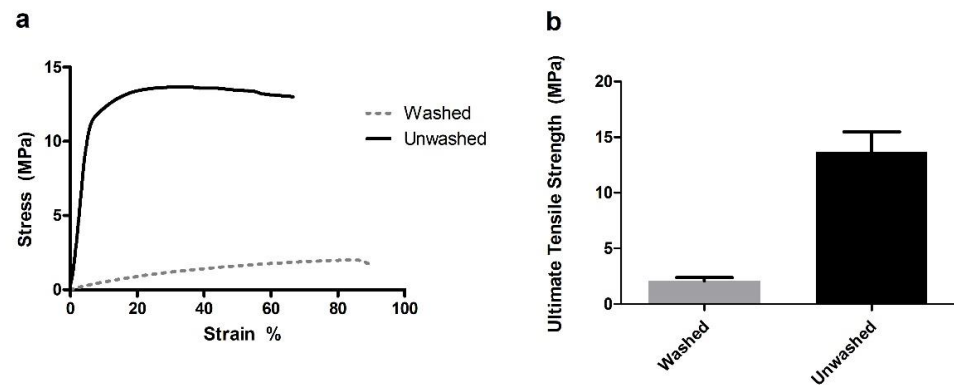

Figure 2. (**a**) Representative tensile data of the Lay-Fomm 60 scaffolds. (**b**) Quantified ultimate tensile strengths for both washed and unwashed Lay-Fomm 60 filaments. Error bars represent ± SD, N = 3.
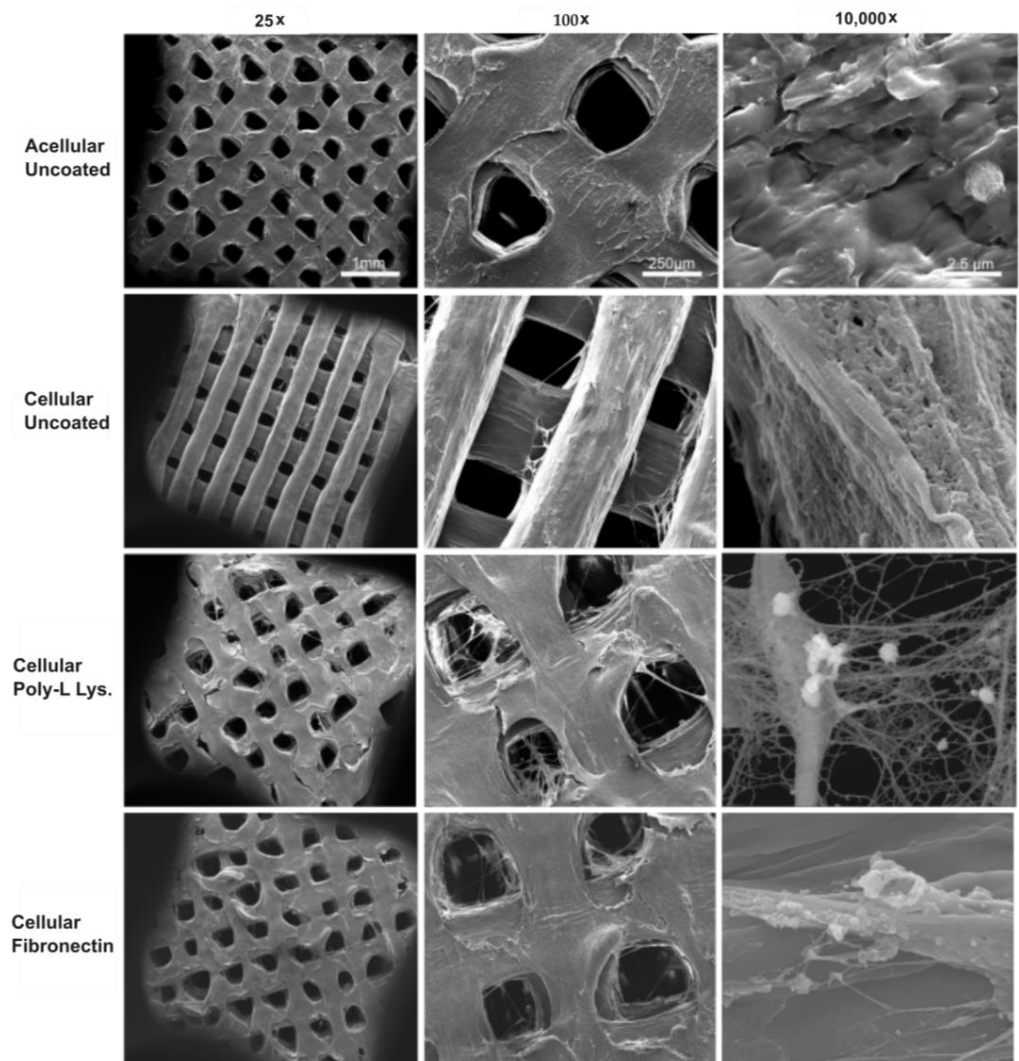

Figure 3. SEM surface morphology of the uncoated and coated scaffolds. Ligament fibroblasts can be observed along the struts and across the pores, signifying that the cells attached to the scaffolds and that the pore size (271.7 ± 4.6 μm) was conducive to cell attachment over 14 days.

Table 3. Mass and μCT characterization of the 3D-printed Lay-Fomm 60 scaffolds.

Property	Value
Dry mass (mg)	88.3 ± 0.7
SV/RV (%)	60.7 ± 1.0
SS (mm^2)	159.5 ± 2.2
SF.Th (μm)	479.9 ± 10.7
SF. Sp (μm)	271.7 ± 4.6
Po. Tot (%)	39.3 ± 1.0

3.2. Cell Isolation, Characterization, and Scaffold Adhesion

Quantitative reverse transcriptase PCR (RT-qPCR) was performed on the primary ligament fibroblasts at passage 0 to assess the baseline ligamentogenic gene expression (Figure 4a). The ligament fibroblasts isolated from the human ACL samples showed a significantly increased expression of ligamentogenic markers collagen type I (2.3 ± 2.9), collagen type III (100.1 ± 128.4), and scleraxis (89.4 ± 101.7) when compared to undifferentiated BMMSCs. This verified isolation and use of the ACL fibroblasts.
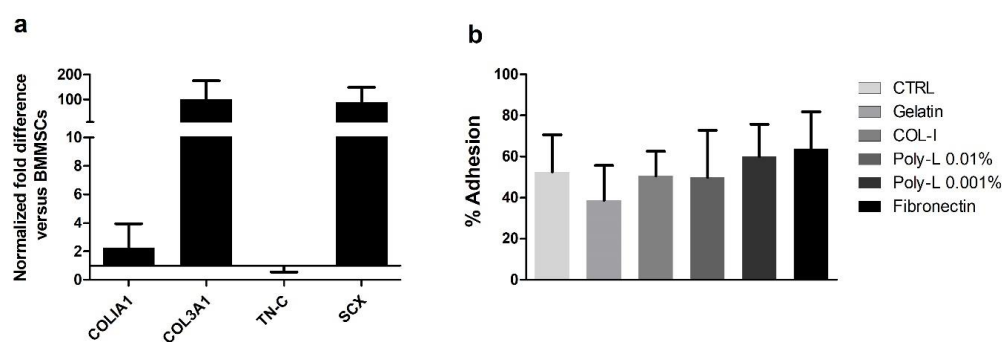

Figure 4. (**a**) Gene expression of the isolated ACL fibroblasts prior to scaffold seeding. The expression levels were normalized to GAPDH with fold difference compared to the passage-0 BMMSCs (N = 3). Error bars represent ± SD. (**b**) Cell attachment of the ligament fibroblasts at day 0 for the uncoated and coated scaffolds. No significant difference was observed between the coated and uncoated conditions.

No significant differences in cell adhesion were observed after seeding onto both the coated and uncoated scaffolds (Figure 4b, $p > 0.05$). The fibronectin-coated scaffolds had the highest adhesion at $63.9 \pm 5.4\%$, while the gelatin-coated ones had the lowest at $38.7 \pm 5.1\%$. The collagen type I-, poly-L-lysine 0.01%-, and poly-L-lysine 0.001%-coated scaffolds displayed cell adhesion of $50.6 \pm 3.6\%$, $49.9 \pm 6.9\%$, and $60.1 \pm 4.7\%$, respectively. The uncoated scaffolds displayed an average cell adhesion of $52.5 \pm 5.7\%$. This indicates that coatings did not significantly improve ligament fibroblast adhesion when compared to the uncoated nanoporous Lay-Fomm 60 scaffolds.

3.3. Cell Viability, Proliferation, and DNA Quantification

Cell metabolic activity for all the cell-seeded scaffolds was measured with the Alamar-Blue™ assay. Figure 5a demonstrates that the fibroblasts seeded on the coated scaffolds were significantly more metabolically active at all timepoints, and plateaus between days 7 and 14. The poly-L-lysine 0.01%-, poly-L-lysine 0.001%, and fibronectin-coated scaffolds had the highest metabolic activity by day 14, culminating in AlamarBlue™ percentage reduction at day 14 of $159.0 \pm 3.5\%$, $156.0 \pm 2.1\%$, and $164.5 \pm 4.5\%$, respectively. This indicates that the scaffolds coated with poly-L-lysine and fibronectin may drive a significantly ($p < 0.001$) higher cell metabolic activity even though they did not significantly increase cell adhesion at day 0.
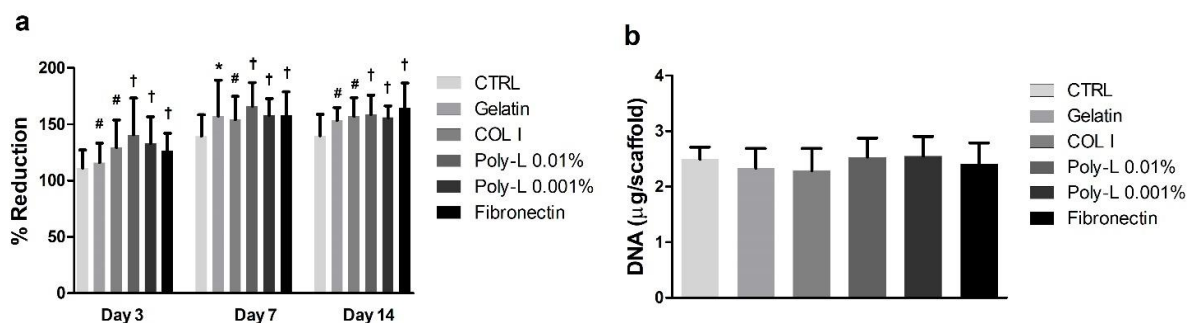
Figure 5. (**a**) Percentage reduction quantified using the AlamarBlue™ assay. Error bars represent ± SD; * = $p < 0.05$, # = $p < 0.005$, and † = $p < 0.0001$. (**b**) DNA quantification per scaffold using a Hoechst 33258 assay. No significant difference was observed between the coated and uncoated conditions.

To confirm whether the increased metabolic activity for various coatings was due to cell growth, total DNA at 14 days was measured. Similar overall growth of ligament fibroblasts was found for the uncoated and coated scaffolds. The uncoated scaffolds contained 2496 ± 71.82 ng DNA per scaffold, and none of the coated scaffolds showed significant differences (Figure 5b). The collagen type I-coated scaffolds on average contained the least DNA at 2.3 ± 0.1 µg DNA, and the poly-L-lysine 0.001%-coated ones contained the most at 2.6 ± 0.1 µg of DNA. The poly-L-lysine 0.01%- and fibronectin-coated scaffolds contained 2.5 ± 0.1 µg and 2.4 ± 0.1 µg DNA, respectively.

Visualization of cell growth and spatial distribution was performed with an inverted light microscope (Zeiss Axiovert 40, Goöttingen, Germany, data not shown). Ligament fibroblasts surrounded and attached to the surface of the scaffold, but also grew into the open pores of all the coated and uncoated scaffolds. Cell viability was assessed with the Live/Dead™ assay (Figure 6). The representative images demonstrate that the number of dead cells in the coated and uncoated scaffolds was negligible in all the cases. The images also show alignment of the adhered cells along the long axis of the scaffold.
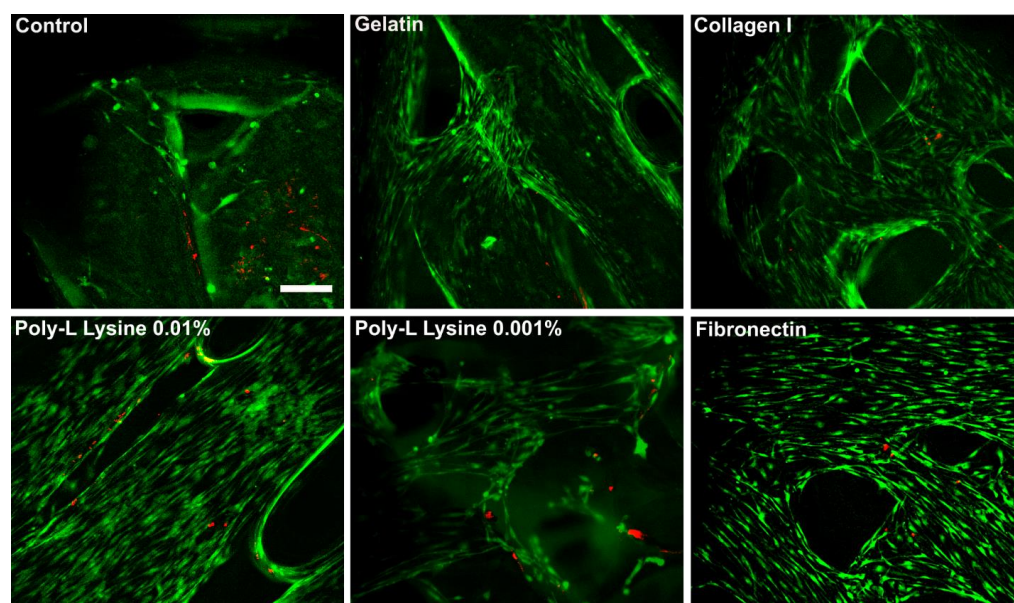

Figure 6. Live/Dead™ staining showing a good viability of ligament fibroblasts on all the scaffolds, coated and uncoated, after 14 days of culture. Live cells stained green, dead cells stained red. Scale bar = 100 µm.

3.4. Ligamentogenic Matrix Formation

Distribution of tenomodulin on the cell-seeded Lay-Fomm 60 scaffolds was assessed using immunofluorescence after 14 days of culture (Figure 7). All the scaffolds displayed some auto-fluorescence, but cells showed specific staining above the acellular background levels on all the coating types. There was an even distribution of ligament-like matrix deposition on the scaffolds, with enhanced tenomodulin (green) deposition on the poly-L-lysine-coated and fibronectin-coated scaffolds. Phalloidin staining (red) was used to demonstrate cell morphology and localization of tenomodulin.
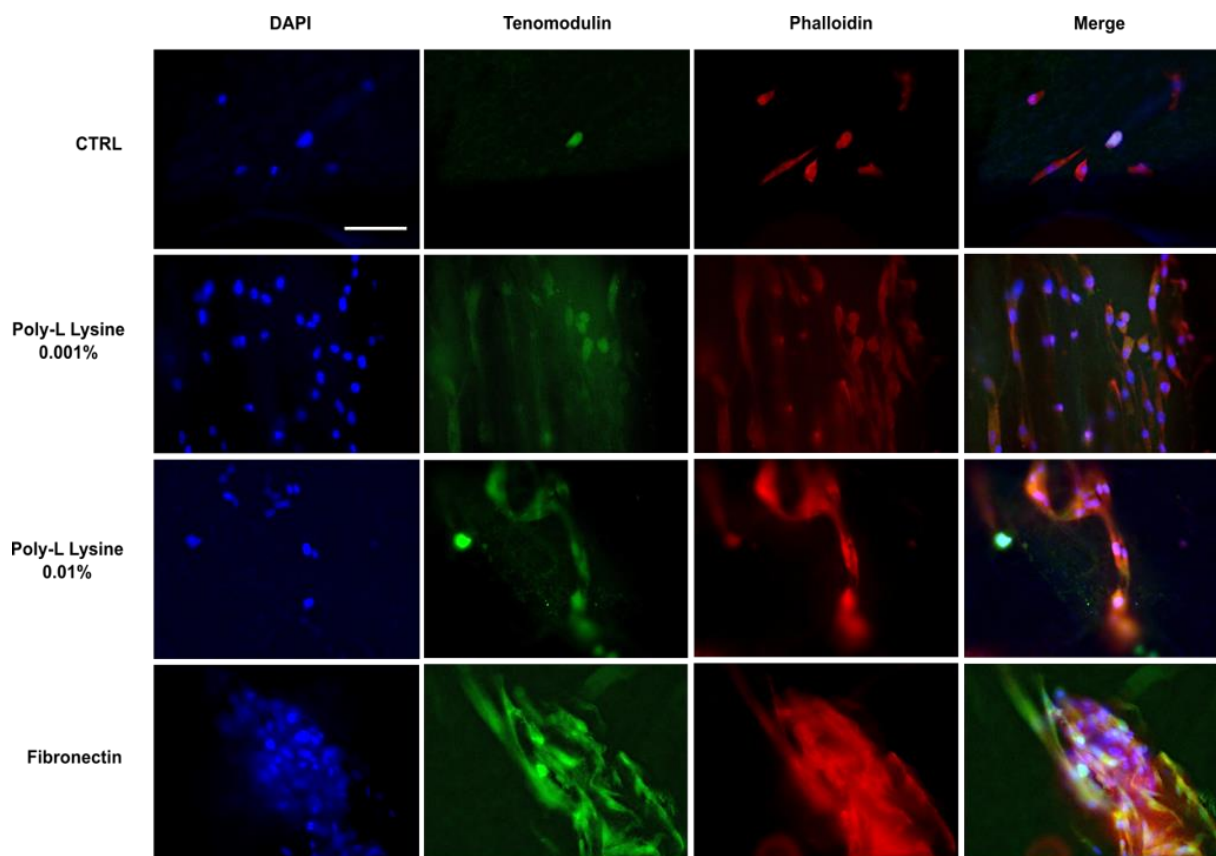

Figure 7. Representative images of tenomodulin and actin fluorescence immunohistology of the ligament fibroblasts cultured on Lay-Fomm 60 for 14 days. The enhanced signal for the poly-L-lysine-coated and fibronectin-coated scaffolds suggests higher tenomodulin deposition on those scaffolds when compared to the uncoated control. Scale bar = 75 μm.

Western blots were performed to assess production of collagen types I and III after 14 days of culture. Densitometry analysis of collagen type I for all the scaffolds showed that the fibroblasts seeded on the collagen- and poly-L-lysine-coated Lay-Fomm 60 scaffolds produced a more extractable—newly synthesized—collagen type I protein, although this was not significantly different from the uncoated control (Figure 8). Production of newly synthesized non-crosslinked collagen type III followed a trend similar to that of collagen type I; the fibroblasts seeded on the collagen- and poly-L-lysine-coated Lay-Fomm 60 scaffolds produced more non-crosslinked collagen type III protein, and both increases in production were significantly different from the control condition. The ratio of extractable collagen type I to collagen type III on the gelatin-coated scaffolds was significantly ($p < 0.05$) lower than the ratio for the uncoated control scaffolds. Use of the other coatings did not otherwise impact the ratio of extractable collagens.
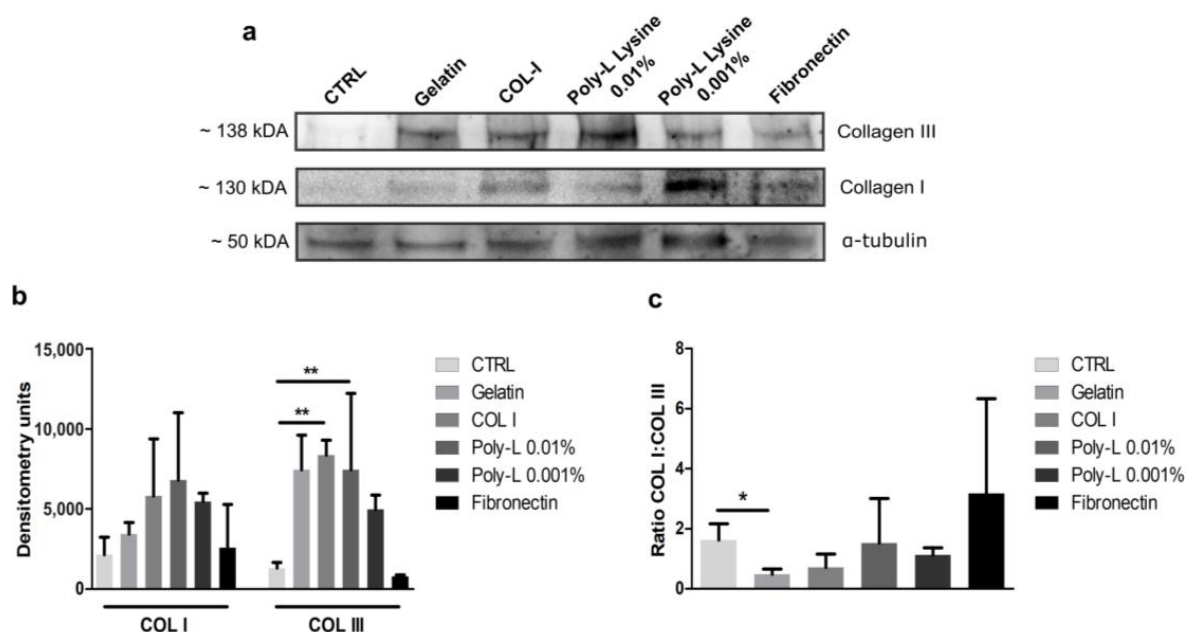
Figure 8. Collagen type I and III analyses of the fibroblast-seeded scaffolds (N = 3). (**a**) Representative Western blot probing extracts for newly synthesized collagen type I, collagen type III, and α-tubulin. (**b**) Densitometry quantification for collagen types I and III deposition on the uncoated and coated scaffolds. (**c**) Ratio of the band densities of extractable collagen type I and collagen type III. Error bars indicate the means ± SD; * = $p < 0.05$ and ** = $p < 0.005$.

4. Discussion

Additive manufacturing is a rapidly expanding field that has found many novel applications in the field of tissue engineering. Generation of personalized anatomic graft substitutes that can replicate the biomechanics of connective tissue has garnered significant momentum in the field of orthopedics during the last two decades. To generate these graft substitutes, various manufacturing methods and synthetic materials have been explored [33,48–55]. While many of the novel scaffolds developed show promise, in vitro cell adherence onto additively manufactured scaffolds remains low [34–37]. There is, therefore, a need to explore ways in which cell adhesion can be improved to enhance tissue regeneration on additively manufactured scaffolds. In this study, we investigated the effect of cell-adhesive coatings on 3D-printed elastomeric scaffolds for ACL tissue engineering. The effect of these coatings on primary human ligament fibroblast adhesion, viability, proliferation, and extracellular matrix deposition was investigated.

The UTS of the Lay-Fomm 60 filament at 2.07 MPa was lower than that of the native tissue (approximately 35 MPa, [56]), but the strain at failure of both the filament and the ACL tissue proved similar [12]. This indicates that Lay-Fomm 60, despite being unsuitable as an ACL substitute alone, may be co-printed with a stiffer extrudable polymer to yield a construct with mechanical properties mimicking those of the ACL. Such composite synthetic scaffolds for ligament tissue engineering have been successfully generated by several groups using manufacturing techniques such as braiding and electrospinning [33,51]. Use of FDM for co-printing presents a cost-effective and reproducible opportunity to fabricate such composites. Micro-CT characterization of Lay-Fomm 60 scaffolds indicates that macropore size and porosity are in line with the optimal values for ligament tissue ingrowth and that the scaffolds were generated with high reproducibility [57,58]. We also demonstrate that ligament fibroblasts grew within pores and that the surface roughness created by the washing of Lay-Fomm 60 may have enhanced adhesion, growth, and proliferation. Thus, the nanoporous washable material, despite showcasing a low UTS, may represent a cost-effective way to generate scaffolds with a surface topology conducive

to enhanced cell adhesion and viability. The co-printing of Lay-Fomm 60 with mechanically competent polylactic acid (PLA) or polyethylene terephthalate glycol (PETG) may yield scaffolds with improved tensile properties.

Use of coatings in this study did not have a significant impact on the ligament fibroblast adhesion at day 0. In fact, only the poly-L-lysine 0.01% and fibronectin coatings showed a marginally higher cell attachment. This indicates that nanoporous Lay-Fomm 60 is just as effective as the other coatings investigated in enhancing ligament fibroblast attachment. This is in line with our previous work on MSC adhesion to Lay-Fomm 60 scaffolds [30]. Use of coatings did impact cell proliferation at all the three measured timepoints. We demonstrate that cell proliferation increased between each time point but that use of coatings led to significantly more cell activity at days 3 and 7. This indicates that while day-14 cell metabolic activity of nanoporous control and coated scaffolds is similar, use of biological coatings may lead to enhanced viability earlier on. Analysis of the DNA content at day 14 also supported this notion. The DNA content was not significantly different at day 14, and thus the nanoporous Lay-Fomm 60 scaffolds performed as well as the coated scaffolds. Live/dead staining also indicated that all the scaffolds supported cell growth and proliferation, but the nanoporous control scaffolds appear to have resulted in more dead cells than the other conditions. Western blot analyses also showed significant matrix formation and indicated that the use of coatings led to increased collagen types I and III deposition at day 14. The scaffold coatings did not, however, increase the ratio of collagen I to collagen III, and the latter was significantly lower than the ratio found in the native ACL tissue (~9:1) for all the samples [59]. Immunohistology qualitatively demonstrated increased tenomodulin deposition on the coated scaffolds. These results may not only signify that the use of coatings such as poly-L-lysine is warranted in maximizing matrix deposition, but also suggests that nanoporous uncoated Lay-Fomm 60 scaffolds alone may represent a viable inexpensive alternative for the tissue engineering of ligament tissue.

Although the scaffolds described herein led to consistent cell adhesion, viability, and matrix deposition, their post-seeding mechanical properties were not considered. They should be considered in future studies to identify whether increased matrix production from ligament fibroblasts seeded on poly-L-lysine-coated scaffolds fosters enhanced tensile properties of the grafts. This might be accomplished through the use of bioreactor culture systems or through in vivo implantation for enhanced tissue maturation prior to ACL reconstruction. Furthermore, a comparison between the coated and uncoated Lay-Fomm 60 scaffolds was performed, but future studies should compare the properties listed above to those of the grafts currently used for surgical reconstruction (i.e., decellularized tendon allografts) to establish whether a nanoporous TPU graft represents an appropriate microenvironment. In future studies, we aim to focus on co-printing, which may lead to more appropriate mechanics.

While the Lay-Fomm 60 scaffolds developed show interesting properties for tissue engineering of the ACL, we believe the characteristics of these biomaterials, such as the ability to be printed in complex geometries, potential resorptive capacities, and biomechanical strength, may prove to be a dynamic and promising alternative in many other smaller and less biomechanically demanding ligament reconstruction scenarios, such as spine, hand, or foot. Additionally, our group has already shown that Lay-Fomm 60 can be used for local drug delivery [45] and mandible bone repair applications [30]. The same method can be used to deliver other biological molecules, such as growth factors. This, paired with the use of mesenchymal stem cells (MSCs), will be further explored as a potentially clinically relevant construct that can mimic ACL and other tissues. Under optimized culture conditions, the material may be well-suited for diverse ligament tissue repair strategies.

There are, however, a few limitations to the study. All the experiments were performed under normoxic and normoglycemic culture conditions. For translational applications, we envision that grafts will be implanted in the joint space, which is relatively hypoxic and hypoglycemic. Thus, future studies will be designed to investigate the cellular interactions of the primary human ligament cells with these 3D-printed coated scaffolds under more

physiological conditions using relative hypoxia and low D-glucose and FBS levels. Future studies will also be designed to assess the ligament cellular interactions with the other cells commonly used for ligament tissue regeneration applications, such as bone marrow-derived stromal cells and adipose stromal cells.

The translatability of this study can be furthered by 3D printing the scaffolds in filamentous geometry with braiding followed by various coating and cell seeding [60,61] to generate implantable grafts for in vivo small animal testing for ACL repair. Another tissue engineering additive manufacturing strategy will be to introduce a biphasic enthesis on both sides of a bioengineered graft to enhance the integration of the graft at the anchorage site [62].

5. Conclusions

In this study, custom nanoporous thermoplastic elastomer scaffolds were generated using commercially available filaments and low-cost desktop 3D printers. This study indicates that the poly-L-lysine-coated Lay-Fomm 60 scaffolds increased ligament fibroblast activity and matrix formation when compared to the uncoated scaffolds but did not have a significant effect on the cell attachment rate and DNA content. This suggests that uncoated Lay-Fomm 60 scaffolds on their own may be viable scaffolds for ligament tissue engineering. Further work will focus on co-printing Lay-Fomm 60 with other extrudable materials in order to generate constructs with more clinically relevant tensile properties and will investigate the use and differentiation of stem cells on Lay-Fomm 60 scaffolds for ligament tissue engineering.

References

1. Majewski, M.; Susanne, H.; Klaus, S. Epidemiology of athletic knee injuries: A 10-year study. *Knee* **2006**, *13*, 184–188. [CrossRef]
2. Kiapour, A.M.; Murray, M.M. Basic science of anterior cruciate ligament injury and repair. *Bone Jt. Res.* **2014**, *3*, 20–31. [CrossRef]
3. Levine, J.W.; Kiapour, A.M.; Quatman, C.E.; Wordeman, S.C.; Goel, V.K.; Hewett, T.E.; Demetropoulos, C.K. Clinically Relevant Injury Patterns After an Anterior Cruciate Ligament Injury Provide Insight Into Injury Mechanisms. *Am. J. Sports Med.* **2012**, *41*, 385–395. [CrossRef] [PubMed]
4. Butler, D.L.; Noyes, F.R.; Grood, E.S. Ligamentous restraints to anterior-posterior drawer in the human knee. A biomechanical study. *J. Bone Jt. Surg. Am.* **1980**, *62*, 259–270. [CrossRef]

5. Campbell, C.J.; Carson, J.D.; Diaconescu, E.D.; Celebrini, R.; Rizzardo, M.R.; Godbout, V.; Fletcher, J.A.; McCormack, R.; Outerbridge, R.; Taylor, T.; et al. Canadian Academy of Sport and Exercise Medicine Position Statement: Neuromuscular Training Programs Can Decrease Anterior Cruciate Ligament Injuries in Youth Soccer Players. *Clin. J. Sport Med.* **2014**, *24*, 263–267. [CrossRef]

6. Gopinathan, P. Fate of the untreated anterior cruciate ligament-injured knee. *J. Orthop.* **2017**, *14*, A1–A3. [CrossRef]

7. Friel, N.A.; Chu, C.R. The Role of ACL Injury in the Development of Posttraumatic Knee Osteoarthritis. *Clin. Sports Med.* **2013**, *32*, 1–12. [CrossRef]

8. Calejo, I.; Costa-Almeida, R.; Reis, R.L.; Gomes, M.E. Enthesis Tissue Engineering: Biological Requirements Meet at the Interface. *Tissue Eng. Part B Rev.* **2019**, *25*, 330–356. [CrossRef] [PubMed]

9. Costa-Paz, M.; Ayerza, M.A.; Tanoira, I.; Astoul, J.; Muscolo, D.L. Spontaneous Healing in Complete ACL Ruptures: A Clinical and MRI Study. *Clin. Orthop. Relat. Res.* **2012**, *470*, 979–985. [CrossRef]

10. Daniel, D.M.; Stone, M.L.; Dobson, B.E.; Fithian, D.C.; Rossman, D.J.; Kaufman, K. Fate of the ACL-injured Patient. *Am. J. Sports Med.* **1994**, *22*, 632–644. [CrossRef]

11. Vavken, P.; Murray, M.M. The Potential for Primary Repair of the ACL. *Sports Med. Arthrosc. Rev.* **2011**, *19*, 44–49. [CrossRef]

12. Murray, M.M. Current Status and Potential of Primary ACL Repair. *Clin. Sports Med.* **2009**, *28*, 51–61. [CrossRef] [PubMed]

13. Andersson, C.; Odensten, M.; Good, L.; Gillquist, J. Surgical or non-surgical treatment of acute rupture of the anterior cruciate ligament. A randomized study with long-term follow-up. *J. Bone Jt. Surg. Am.* **1989**, *71*, 965–974. [CrossRef]

14. Woo, S.L.-Y.; Chan, S.S.; Yamaji, T. Biomechanics of knee ligament healing, repair and reconstruction. *J. Biomech.* **1997**, *30*, 431–439. [CrossRef]

15. Murray, M.M. History of ACL Treatment and Current Gold Standard of Care. In *The ACL Handbook: Knee Biology, Mechanics, and Treatment*; Murray, M.M., Vavken, P., Fleming, B., Murray, M.M., Vavken, P., Fleming, B., Eds.; Springer: New York, NY, USA, 2013; pp. 19–28. [CrossRef]

16. Björnsson, H.; Samuelsson, K.; Sundemo, D.; Desai, N.; Sernert, N.; Rostgård-Christensen, L.; Karlsson, J.; Kartus, J. A Randomized Controlled Trial With Mean 16-Year Follow-up Comparing Hamstring and Patellar Tendon Autografts in Anterior Cruciate Ligament Reconstruction. *Am. J. Sports Med.* **2016**, *44*, 2304–2313. [CrossRef] [PubMed]

17. Ahn, J.H.; Kim, J.G.; Wang, J.H.; Jung, C.H.; Lim, H.C. Long-Term Results of Anterior Cruciate Ligament Reconstruction Using Bone–Patellar Tendon–Bone: An Analysis of the Factors Affecting the Development of Osteoarthritis. *Arthrosc. J. Arthrosc. Relat. Surg.* **2012**, *28*, 1114–1123. [CrossRef] [PubMed]

18. Selmi, T.A.S.; Fithian, D.; Neyret, P. The evolution of osteoarthritis in 103 patients with ACL reconstruction at 17 years follow-up. *Knee* **2006**, *13*, 353–358. [CrossRef] [PubMed]

19. Barenius, B.; Ponzer, S.; Shalabi, A.; Bujak, R.; Norlén, L.; Eriksson, K. Increased Risk of Osteoarthritis After Anterior Cruciate Ligament Reconstruction. *Am. J. Sports Med.* **2014**, *42*, 1049–1057. [CrossRef]

20. Woo, S.L.-Y.; Wu, C.; DeDe, O.; Vercillo, F.; Noorani, S. Biomechanics and anterior cruciate ligament reconstruction. *J. Orthop. Surg. Res.* **2006**, *1*, 2. [CrossRef]

21. Herrington, L.; Wrapson, C.; Matthews, M.; Matthews, H. Anterior Cruciate Ligament reconstruction, hamstring versus bone–patella tendon–bone grafts: A systematic literature review of outcome from surgery. *Knee* **2005**, *12*, 41–50. [CrossRef]

22. Oluwadamilola, A.; Yousaf, S.; Zare, M.; Mozafari, M.; Youseffi, M.; Twigg, P.; Sefate, F. 14—Scaffolds for ligament tissue engineering. In *Handbook of Tissue Engineering Scaffolds: Volume One*; Mozafari, M., Sefat, F., Atala, A., Mozafari, M., Sefat, F., Atala, A., Eds.; 2019; pp. 299–327. Available online: http://www.sciencedirect.com/science/article/pii/B9780081025635000149 (accessed on 4 August 2022).

23. Gentleman, E.; Lay, A.N.; Dickerson, D.A.; Nauman, E.A.; Livesay, G.A.; Dee, K.C. Mechanical characterization of collagen fibers and scaffolds for tissue engineering. *Biomaterials* **2003**, *24*, 3805–3813. [CrossRef]

24. Laurent, C.; Liu, X.; De Isla, N.; Wang, X.; Rahouadj, R. Defining a scaffold for ligament tissue engineering: What has been done, and what still needs to be done. *J. Cell. Immunother.* **2018**, *4*, 4–9. [CrossRef]

25. Woo, S.L.-Y.; Hollis, J.M.; Adams, D.J.; Lyon, R.M.; Takai, S. Tensile properties of the human femur-anterior cruciate ligament-tibia complex: The effects of specimen age and orientation. *Am. J. Sports Med.* **1991**, *19*, 217–225. [CrossRef] [PubMed]

26. Ahangar, P.; Cooke, M.E.; Weber, M.H.; Rosenzweig, D.H. Current Biomedical Applications of 3D Printing and Additive Manufacturing. *Appl. Sci.* **2019**, *9*, 1713. [CrossRef]

27. Calore, A.R.; Sinha, R.; Harings, J.; Bernaerts, K.V.; Mota, C.; Moroni, L. Additive Manufacturing Using Melt Extruded Thermoplastics for Tissue Engineering. *Methods Mol. Biol. Clifton NJ* **2021**, *2147*, 75–99. [CrossRef]

28. Diegel, O. 10.02—Additive Manufacturing: An Overview. In *Comprehensive Materials Processing*; Hashmi, S., Batalha, G.F., Van Tyne, C.J., Yilbas, B., Hashmi, S., Batalha, G.F., Van Tyne, C.J., Yilbas, B., Eds.; Elsevier B.V.: Oxford, UK, 2014; pp. 3–18. Available online: http://www.sciencedirect.com/science/article/pii/B9780080965321010001 (accessed on 2 September 2020).

29. Haglund, L.; Ahangar, P.; Rosenzweig, D.H. Advancements in 3D printed scaffolds to mimic matrix complexities for musculoskeletal repair. *Curr. Opin. Biomed. Eng.* **2019**, *10*, 142–148. [CrossRef]

30. Cooke, M.E.; Ramirez-Garcialuna, J.L.; Rangel-Berridi, K.; Park, H.; Nazhat, S.N.; Weber, M.H.; Henderson, J.E.; Rosenzweig, D.H. 3D Printed Polyurethane Scaffolds for the Repair of Bone Defects. *Front. Bioeng. Biotechnol.* **2020**, *8*, 557215. [CrossRef] [PubMed]

31. Leong, N.L.; Kabir, N.; Arshi, A.; Nazemi, A.; Wu, B.; Petrigliano, F.A.; McAllister, D.R. Evaluation of Polycaprolactone Scaffold with Basic Fibroblast Growth Factor and Fibroblasts in an Athymic Rat Model for Anterior Cruciate Ligament Reconstruction. *Tissue Eng. Part A* **2015**, *21*, 1859–1868. [CrossRef]

32. Podporska-Carroll, J.; Ip, W.Y.; Gogolewski, S. Biodegradable poly(ester urethane) urea scaffolds for tissue engineering: Interaction with osteoblast-like MG-63 cells. *Acta Biomater.* **2014**, *10*, 2781–2791. [CrossRef]

33. Vaquette, C.; Kahn, C.; Frochot, C.; Nouvel, C.; Six, J.-L.; De Isla, N.; Luo, L.-H.; Cooper-White, J.; Rahouadj, R.; Wang, X. Aligned poly(L-lactic-co-e-caprolactone) electrospun microfibers and knitted structure: A novel composite scaffold for ligament tissue engineering. *J. Biomed. Mater. Res. Part A* **2010**, *94*, 1270–1282. [CrossRef]

34. Kimura, Y.; Hokugo, A.; Takamoto, T.; Tabata, Y.; Kurosawa, H. Regeneration of Anterior Cruciate Ligament by Biodegradable Scaffold Combined with Local Controlled Release of Basic Fibroblast Growth Factor and Collagen Wrapping. *Tissue Eng. Part C Methods* **2008**, *14*, 47–57. [CrossRef] [PubMed]

35. Hutmacher, D.W.; Schantz, T.; Zein, I.; Ng, K.W.; Teoh, S.H.; Tan, K.C. Mechanical properties and cell cultural response of polycaprolactone scaffolds designed and fabricated via fused deposition modeling. *J. Biomed. Mater. Res.* **2001**, *55*, 203–216. [CrossRef] [PubMed]

36. Youssef, A.; Hollister, S.J.; Dalton, P.D. Additive manufacturing of polymer melts for implantable medical devices and scaffolds. *Biofabrication* **2017**, *9*, 012002. [CrossRef]

37. Sahoo, S.; Ouyang, H.; Goh, J.C.-H.; Tay, T.-E.; Toh, S. Characterization of a Novel Polymeric Scaffold for Potential Application in Tendon/Ligament Tissue Engineering. *Tissue Eng.* **2006**, *12*, 91–99. [CrossRef] [PubMed]

38. Deepthi, S.; Sundaram, M.N.; Kadavan, J.D.; Jayakumar, R. Layered chitosan-collagen hydrogel/aligned PLLA nanofiber construct for flexor tendon regeneration. *Carbohydr. Polym.* **2016**, *153*, 492–500. [CrossRef]

39. Domingos, M.; Intranuovo, F.; Gloria, A.; Gristina, R.; Ambrosio, L.; Bártolo, P.; Favia, P. Improved osteoblast cell affinity on plasma-modified 3-D extruded PCL scaffolds. *Acta Biomater.* **2013**, *9*, 5997–6005. [CrossRef]

40. Poh, P.S.; Hutmacher, D.W.; Holzapfel, B.M.; Solanki, A.K.; Stevens, M.M.; Woodruff, M.A. In vitro and in vivo bone formation potential of surface calcium phosphate-coated polycaprolactone and polycaprolactone/bioactive glass composite scaffolds. *Acta Biomater.* **2016**, *30*, 319–333. [CrossRef]

41. Sousa, I.; Mendes, A.; Pereira, R.F.; Bártolo, P.J. Collagen surface modified poly(ε-caprolactone) scaffolds with improved hydrophilicity and cell adhesion properties. *Mater. Lett.* **2014**, *134*, 263–267. [CrossRef]

42. Wang, W.; Caetano, G.; Ambler, W.S.; Blaker, J.J.; Frade, M.A.; Mandal, P.; Diver, C.; Bártolo, P. Enhancing the Hydrophilicity and Cell Attachment of 3D Printed PCL/Graphene Scaffolds for Bone Tissue Engineering. *Materials* **2016**, *9*, 992. [CrossRef]

43. You, J.; Preen, R.J.; Bull, L.; Greenman, J.; Ieropoulos, I. 3D printed components of microbial fuel cells: Towards monolithic microbial fuel cell fabrication using additive layer manufacturing. *Sustain. Energy Technol. Assess.* **2017**, *19*, 94–101. [CrossRef]

44. Tsai, K.J.; Dixon, S.; Hale, L.R.; Darbyshire, A.; Martin, D.; de Mel, A. Biomimetic heterogenous elastic tissue development. *NPJ Regen. Med.* **2017**, *2*, 16. [CrossRef]

45. Ahangar, P.; Akoury, E.; Luna, A.S.R.G.; Nour, A.; Weber, M.H.; Rosenzweig, D.H. Nanoporous 3D-Printed Scaffolds for Local Doxorubicin Delivery in Bone Metastases Secondary to Prostate Cancer. *Materials* **2018**, *11*, 1485. [CrossRef]

46. Fairag, R.; Rosenzweig, D.H.; Garcialuna, J.L.R.; Weber, M.H.; Haglund, L. Three-Dimensional Printed Polylactic Acid Scaffolds Promote Bone-like Matrix Deposition in Vitro. *ACS Appl. Mater. Interfaces* **2019**, *11*, 15306–15315. [CrossRef]

47. Pitaru, A.A.; Lacombe, J.-G.; Cooke, M.E.; Beckman, L.; Steffen, T.; Weber, M.H.; Martineau, P.A.; Rosenzweig, D.H. 3D Printing to Microfabricate Stiff and Elastic Scaffolds that Mimic Ligament Tissue. *Micromachines* **2020**, *11*, 846. [CrossRef] [PubMed]

48. Ramirez-Garcia-Luna, J.L.; Wong, T.H.; Chan, D.; Al-Saran, Y.; Awlia, A.; Abou-Rjeili, M.; Ouellet, S.; Akoury, E.; Lemarié, C.A.; Henderson, J.E.; et al. Defective bone repair in diclofenac treated C57Bl6 mice with and without lipopolysaccharide induced systemic inflammation. *J. Cell. Physiol.* **2018**, *234*, 3078–3087. Available online: https://onlinelibrary.wiley.com/doi/full/10.1002/jcp.27128 (accessed on 2 September 2020). [CrossRef]

49. Park, H.; Cooke, M.E.; Lacombe, J.-G.; Weber, M.H.; Martineau, P.A.; Nazhat, S.N.; Rosenzweig, D.H. Continuous Two-Zone In Vitro Co-culture Model of the Enthesis. *Biomed. Mater. Devices* **2022**, 1–10. Available online: https://link.springer.com/article/10.1007/s44174-022-00015-2 (accessed on 7 April 2023). [CrossRef]

50. Park, H.; Nazhat, S.N.; Rosenzweig, D.H. Mechanical activation drives tenogenic differentiation of human mesenchymal stem cells in aligned dense collagen hydrogels. *Biomaterials* **2022**, *286*, 121606. [CrossRef]

51. Ciucci, A.; Zannoni, G.F.; Buttarelli, M.; Lisi, L.; Travaglia, D.; Martinelli, E.; Scambia, G.; Gallo, D. Multiple direct and indirect mechanisms drive estrogen-induced tumor growth in high grade serous ovarian cancers. *Oncotarget* **2016**, *7*, 8155–8171. [CrossRef] [PubMed]

52. Chen, Y.-Y.; He, S.-T.; Yan, F.-H.; Zhou, P.-F.; Luo, K.; Zhang, Y.-D.; Xiao, Y.; Lin, M.-K. Dental pulp stem cells express tendon markers under mechanical loading and are a potential cell source for tissue engineering of tendon-like tissue. *Int. J. Oral Sci.* **2016**, *8*, 213–222. [CrossRef] [PubMed]

53. He, J.; Jiang, N.; Qin, T.; Zhang, W.; Liu, Z.; Liu, Y.; Li, D. Microfiber-reinforced nanofibrous scaffolds with structural and material gradients to mimic ligament-to-bone interface. *J. Mater. Chem. B* **2017**, *5*, 8579–8590. [CrossRef]

54. Chen, X.; Qi, Y.-Y.; Wang, L.-L.; Yin, Z.; Yin, G.-L.; Zou, X.-H.; Ouyang, H.-W. Ligament regeneration using a knitted silk scaffold combined with collagen matrix. *Biomaterials* **2008**, *29*, 3683–3692. [CrossRef] [PubMed]

55. Wu, S.; Wang, Y.; Streubel, P.N.; Duan, B. Living nanofiber yarn-based woven biotextiles for tendon tissue engineering using cell tri-culture and mechanical stimulation. *Acta Biomater.* **2017**, *62*, 102–115. [CrossRef] [PubMed]

56. Takeda, Y.; Xerogeanes, J.W.; Livesay, G.A.; Fu, F.H.; Woo, S.L.-Y. Biomechanical function of the human anterior cruciate ligament. *Arthrosc. J. Arthrosc. Relat. Surg.* **1994**, *10*, 140–147. [CrossRef]

57. Rao, R.; Libring, S.; Fleisher, E.; Yankannah, Y.; Freeman, J.W. Design and characterization of three-dimensional twist-braid scaffolds for anterior cruciate ligament regeneration. *Technology* **2017**, *5*, 98–106. [CrossRef]

58. Cooper, J.A.; Lu, H.H.; Ko, F.K.; Freeman, J.W.; Laurencin, C.T. Fiber-based tissue-engineered scaffold for ligament replacement: Design considerations and in vitro evaluation. *Biomaterials* **2005**, *26*, 1523–1532. [CrossRef]

59. Duthon, V.L.A.; Barea, C.; Abrassart, S.; Fasel, J.H.; Fritschy, D.; Menetrey, J. Anatomy of the anterior cruciate ligament. *Knee Surg. Sports Traumatol. Arthrosc.* **2005**, *14*, 204–213. [CrossRef] [PubMed]

60. Li, L.; Hao, R.; Qin, J.; Song, J.; Chen, X.; Rao, F.; Zhai, J.; Zhao, Y.; Zhang, L.; Xue, J. Electrospun Fibers Control Drug Delivery for Tissue Regeneration and Cancer Therapy. *Adv. Fiber Mater.* **2022**, *4*, 1375–1413. [CrossRef]

61. Peixoto, T.; Carneiro, S.; Fangueiro, R.; Guedes, R.M.; Paiva, M.C.; Lopes, M.A. Engineering hybrid textile braids for tendon and ligament repair application. *J. Appl. Polym. Sci.* **2021**, *139*, 52013. Available online: https://onlinelibrary.wiley.com/doi/abs/10.1002/app.52013 (accessed on 7 April 2023). [CrossRef]

62. Chen, C.; Shi, Q.; Li, M.; Chen, Y.; Zhang, T.; Xu, Y.; Liao, Y.; Ding, S.; Wang, Z.; Li, X.; et al. Engineering an enthesis-like graft for rotator cuff repair: An approach to fabricate highly biomimetic scaffold capable of zone-specifically releasing stem cell differentiation inducers. *Bioact. Mater.* **2022**, *16*, 451–471. [CrossRef]